JOURNAL OF GEOPHYSICAL RESEARCH, VOL. 115, D00K15, doi:10.1029/2009JD013273, 2010

Dust aerosol vertical structure measurements using three MPL lidars during 2008 China-U.S. joint dust field experiment

Zhongwei Huang,[1] Jianping Huang,[1] Jianrong Bi,[1] Guoyin Wang,[1] Wencai Wang,[1] Qiang Fu,[2] Zhanqing Li,[3] Si-Chee Tsay,[4] and Jinsen Shi[1]

Received 28 September 2009; revised 31 January 2010; accepted 5 April 2010; published 30 July 2010.

[1] The 2008 China-U.S. joint dust field experiment, which aims to estimate the effect of dust on radiative forcing and its associated climatic impacts, was conducted during the dust-intensive period from March to June of 2008 over the Loess Plateau of northwest China. Dust aerosol vertical profiles and long-range transport of dust storm were measured with the three MPL-net Micro-Pulse Lidar (MPL) systems as well as other ground-based instruments and spaceborne remote sensing techniques. In this study, to ensure the effectiveness of the retrieval results, an effective algorithm was introduced for retrieving aerosol optical properties and vertical profiles from Mie lidar measurements. The advantage of this algorithm is that Aerosol Optical Depth (AOD) retrieval from lidar measurements can be accomplished without the use of the so-called lidar ratio for the corresponding quantities obtained from the AERONET Sun photometer. Dust aerosol vertical profiles are derived successfully from three MPL lidar systems using this algorithm. A dust storm that affected a large part of northwest China on 2 May 2008 was studied using measurements obtained from the three ground-based lidar systems, satellite-borne instruments and NCEP reanalysis data. The results show that different aerosol vertical structures were present at each site, and the colder Siberia air mass and stronger and longer cyclones around Mongolia are key features leading to the dust storm.

Citation: Huang, Z., J. Huang, J. Bi, G. Wang, W. Wang, Q. Fu, Z. Li, S.-C. Tsay, and J. Shi (2010), Dust aerosol vertical structure measurements using three MPL lidars during 2008 China-U.S. joint dust field experiment, *J. Geophys. Res.*, *115*, D00K15, doi:10.1029/2009JD013273.

1. Introduction

[2] The vertical distribution of dust aerosols is a critical problem in estimating the effect of dust on radiative forcing and its associated climatic impacts [*Claquin et al.*, 1998; *Zhu et al.*, 2007; *Forster et al.*, 2007; *Huang et al.*, 2009]. An analysis of observations by *Minnis and Cox* [1978] and a model study by *Carlson and Benjamin* [1980] both indicated that an elevated Saharan dust layer could change the atmospheric heating rate dramatically. According to *Liao and Seinfeld* [1998], clear-sky long-wave radiative forcing and cloudy-sky top-of-atmosphere (TOA) short-wave (SW) radiative forcing are very sensitive to the altitude of a dust layer. *Meloni et al.* [2005] found that SW aerosol radiative forcing at TOA is strongly dependent on aerosol vertical profiles. Substantial magnitude and large uncertainties were found for aerosol radiative forcing in some heavily polluted regions [*Li*, 1998; *Satheesh and Ramanathan*, 2000; *Huang et al.*, 2008c; *Zhang et al.*, 2007]. *Ramanathan et al.* [2001] suggested that a combination of the aerosol direct and indirect effects could weaken the hydrological cycle, which could be a major environmental issue during this century.

[3] Therefore, knowledge of the actual variations in aerosol spatial and temporal distributions will facilitate the solution of problems pertaining to the estimation of dust radiative forcing, as well as those concerned with climatology and climate change. In particular, LIDAR offers some remarkable advantages for accurately determining the vertical structure of dust aerosols and their related optical properties [*Lü et al.*, 1977; *Zhou et al.*, 1998; *Qiu et al.*, 2003; *He and Mao*, 2004; *Hua et al.*, 2004; *Sugimoto et al.*, 2006]. To better understand and quantify dust aerosol radiative forcing and to reduce the uncertainty of its climatic effect, a large-scale China-U.S. joint dust field experiment was carried out in China in 2008 (Z. Li et al., Overview of the East Asian Study of Tropospheric Aerosols and Impact on Regional Climate (EAST-AIRC), manuscript in preparation, 2010) following the success of a similar but smaller-scale pilot experiment [*Li et al.*, 2007]. A major subexperiment was carried out over the Loess Plateau (a unique semi-arid land surface to study

[1]Key Laboratory for Semi-Arid Climate Change of the Ministry of Education, College of Atmospheric Sciences, Lanzhou University, Lanzhou, China.
[2]Department of Atmospheric Science, University of Washington, Seattle, Washington, USA.
[3]Department of Atmospheric and Oceanic Science, University of Maryland, College Park, Maryland, USA.
[4]NASA Goddard Space Flight Center, Greenbelt, Maryland, USA.

0148-0227/10/2009JD013273

dust aerosols in Northwest China) from March to June. *Huang et al.* [2008c] suggested that changes in climate and climate variability will likely have a significant impact on sensitive arid and semi-arid areas, such as the Loess Plateau. Severe drought and desertification in this area could, in turn, have a profound influence on atmospheric circulation, the East Asian monsoon, global climate, and climate change. Consequently, information on the Loess Plateau is of great importance, but little is currently available in the literature [*Guan et al.*, 2009]. Likewise, before the present investigation, hardly any consideration was given to using LIDAR observations to measure the vertical structure of dust aerosols over Northwest China.

[4] Dust aerosol vertical profiles were measured with three MPL systems during the 2008 China-U.S. joint dust field experiment (March–June 2008). Furthermore, three MPL join measurements will benefit for us to investigate characteristics of long-range transport of dust storm events. Unfortunately, the limitations of the Mie lidar measurements are due to the fact that only one set of signals is measured while two sets of parameters, backscatter and extinction, determine the signal. Many works about how to better retrieve lidar data have been introduced in the literature [*Kohl*, 1978; *Potter*, 1987; *Klett*, 1981; *Kovalev*, 1993; *Roy et al.*, 1993; *Ackermann*, 1997]. One of reliable works was suggested by *Welton* [1998], however, AOD from co-located Sun photometer or sky radiometer measurements is essential. Here, a more effective method that use lidar-retrieved AOD from so-called transmission method, which theoretical basis, advantages and limitations of this method have been well studied [*Young*, 1995; *Stephens et al.*, 2001; *Chand et al.*, 2008; *Esselborn et al.*, 2008], is used to retrieve aerosol optical properties from lidar measurements during the joint dust field experiment. In this paper, we will discuss the detail process of retrieval algorithm and focus on analysis of dust aerosol vertical structure over Northwest China. Our MPL measurements should lead to a reliable analysis of dust aerosol vertical structure and expand our understanding of the impact of aerosols on climate.

[5] The 2008 China-U.S. joint dust field experiment and the various instruments used during the experiment are introduced in Section 2. The algorithm for retrieving aerosol optical properties is introduced in Section 3 and validated in Section 4. The information obtained on the dust storm that affected a large part of Northwest China on 2 May 2008 is presented in Section 5. Finally, the characteristics of the aerosol vertical structure over Northwest China in the spring are described in Section 6.

2. Measurements and Data

[6] The 2008 China-U.S. joint dust field experiment aims to attain a better understanding of the complex and unique aerosol (especially for dust aerosol) climatic effects which impact cloud reflectivity and precipitation processes in the east-Asia region to the earth's climate and environment. One of these stations is located at a permanent site (the Semi-Arid Climate and Environment Observatory of Lanzhou University (SACOL) in Yuzhong, 35.95°N, 104.1°E) [*Huang et al.*, 2008b], another at SACOL's Mobile Facility (SMF, deployed in Jintai, 37.57°N, 104.23°E), and the third at the U.S. Department of Energy Atmospheric Radiation Measurements (ARM) Ancillary Facility (AAF mobile laboratories SMART-COMMIT, deployed in Zhangye, 39.08°N, 100.27°E), was conducted by Lanzhou University, University of Maryland (USA) and Institute of Atmospheric Physics (CAS, China) during the dust-intensive observation period from March to June of 2008 over the Loess Plateau of Northwest China. The observations were made via an assortment of instruments, including LIDAR, AERONET CIMEL Sun photometer, radiometer, TSI Integrating Nephelometer, Total Sky Imager (Model 880), pyranometers, MultiFilter Rotating Shadowband Radiometer (MFR-SR), Andersen sampler, and basic meteorological observation and so on. Three MPL-net lidars play a vital role in the joint dust field experiment not only simultaneously observe spatial and temporal changes of dust aerosol vertical structure but also investigate the characteristics of long-range transport of dust events. Combining with other ground-based instruments and space-borne remote sensing techniques, measurements of the three-dimension construction of dust storm has been developed and analyzed quantitatively. Some of the instruments used to in this study will now be described.

2.1. MPL System

[7] MPL lidar is a safe, compact, and maintenance-free lidar system originally developed by *Spinhirne* [1993] for acquiring long-term data sets of backscatter profiles of aerosols and clouds [*Welton et al.*, 2001]. The system consists of a laser power supply, a signal control unit, a telescope that serves as both the transmitter for laser transmissions and the receiver for return signals, and a laptop computer for data acquisition and display [*Powell et al.*, 2000; *Campbell et al.*, 2002]. MPL uses an Nd: YLF pulsed laser diode, operating at a wavelength of 527 nm. The continual aerosol and cloud measurements are acquired with a 75-m range resolution and a 1-min time average. Three MPLs were employed for measurements of dust vertical structure and the characteristics of long-range transport of dust events in this study.

2.2. AERONET Sun Photometer

[8] The Cimel-Electronique CE-318 Sun photometer (the AERONET network standard instrument) is an automatic direct solar and sky radiometer, with spectral interference filters (10 nm FWHM) centered in the wavelengths selected for aerosol measurements, 440, 670, 870, and 1020 nm [*Carlos et al.*, 2006]. Direct sun measurements are performed at these wavelengths to determine AOD, and another channel (at 940 nm) is used for water vapor content retrieval. Cimel Sun photometers are calibrated annually by comparison with an AERONET master instrument. For more details about this instrument, you may refer to *Holben et al.* [1998]. The maximum AERONET uncertainty in AOD retrieval is estimated to be 0.02 [*Eck et al.*, 1999]. The AODs from the AERONET Sun photometer are converted at a wavelength of 527 nm, which matches the laser wavelength using the 440-nm and 670-nm measurements, in accordance with the Ångström formula [*Ångström*, 1929, 1930; *Cachorro et al.*, 1987].

2.3. Cloud-Aerosol Lidar With Orthogonal Polarization

[9] Cloud-Aerosol Lidar With Orthogonal Polarization (CALIOP) which is on board the Cloud-Aerosol Lidar and

Infrared Pathfinder Satellite Observations (CALIPSO) satellite is designed to acquire vertical profiles of elastic backscatter at two wavelengths (532 nm and 1064 nm) from a near nadir-viewing geometry during both day and night phases of the orbit. In addition to total backscatter at the two wavelengths, CALIOP also provides profiles of linear depolarization at 532 nm. The depolarization measurements enable the discrimination between ice and water clouds, and the identification of non-spherical aerosol particles [*Winker et al.*, 2007; *Huang et al.*, 2007]. CALIOP's high resolution vertical profiling ability and accurate depolarization measurements make it a superb platform for the study of dust aerosols [*Liu et al.*, 2008a, 2008b]. In this study, CALIOP level 1 data are used to help us analyze vertical profiles of dust storm event.

2.4. Aura/Ozone Monitoring Instrument

[10] The Aura/Ozone Monitoring Instrument (Aura/OMI) employs hyperspectral imaging in a push-broom mode to observe solar backscatter radiation in the visible [350–500 nm) and ultraviolet (UV-1, 270–314 nm, UV-2 306–380 nm) ranges, with a 0.0–0.45 nm FWHM spectral resolution. Dust aerosols absorb a significant amount of light at short wavelengths, as they consist primarily of crustal elements such as silicon, aluminum, iron, calcium, and magnesium [*Claquin et al.*, 1999; *Sokolik and Toon*, 1996]. The OMI can be used in conjunction with the Aerosol Index (AI) concept, developed by *Torres et al.* [1998] based on TOMS observations in the near ultraviolet range, to distinguish dust from other aerosol types by its high absorption properties [*Torres et al.*, 2002, 2007]. In the present study, Aura/OMI AI results could be used to describe the influencing intensity and transport path of a dust storm.

3. Retrieval Method

[11] The lidar range-corrected backscatter signal can be written as [*Measures*, 1984; *Fernald et al.*, 1972],

$$X(z) = CE\beta(z)\exp\left(-2\int_0^z \sigma(z')dz'\right), \tag{1}$$

where z is the distance between the particles and the lidar unit, C is the lidar system calibration constant, E is the laser pulse energy, $\beta(z)$ is the atmospheric volume backscattering coefficient, and $d(z)$ is the atmospheric volume extinction coefficient which is related to the total optical depth by

$$\tau(z) = \int_0^z \sigma(z')dz'. \tag{2}$$

[12] The atmosphere can be considered as the sum of its air molecules and aerosol components, and the lidar range-corrected backscatter signal is then given by

$$X(z) = CE[\beta_a(z) + \beta_m(z)]\exp\left(-2\int_0^z [\sigma_a(z') + \sigma_m(z')]dz'\right), \tag{3}$$

where the subscripts a and m denote aerosol and air molecule, respectively. Unfortunately, the retrieval of aerosol backscattering and extinction profiles from single-wavelength lidar measurements is complicated by the fact that the lidar equation contains two unknowns: The backscattering and extinction coefficients. In order to obtain an analytical solution to the lidar equation, it has been a common practice to assume that these parameters are related by the extinction-to-backscatter ratio, or lidar ratio [*Fernald*, 1984]. The relationships between the volume extinction coefficient and the backscattering coefficient can be written as

$$\mathrm{S_a} = \sigma_\mathrm{a}(\mathrm{z})/\beta_\mathrm{a}(\mathrm{z}), \mathrm{S_m} = \sigma_\mathrm{m}(\mathrm{z})/\beta_\mathrm{m}(\mathrm{z}).$$

[13] The air molecule ratio $\mathrm{S_m}$ has a constant value of $8\Pi/3$, whereas the aerosol lidar ratio ($\mathrm{S_a}$) always varies, depending on the aerosol size distribution and particle refractive index and so on [*Reagan et al.*, 1988; *Franke et al.*, 2001].

[14] Errors caused by the lidar ratio when retrieving aerosol optical properties are typically very obvious, especially those pertaining to the aerosol extinction coefficient and AOD [*Measures*, 1984]. In this study, an algorithm is introduced for retrieving AOD without using the lidar ratio. For a region in which no aerosol is present (air molecules only), equation (3) can be written as

$$X(z) = CE\beta_m(z)\exp\left(-2\int_0^z [\sigma_a(z') + \sigma_m(z')]dz'\right). \tag{4}$$

[15] If the portion of such a region lying between the altitudes Z_b and Z_t is selected, the lidar range-corrected backscatter signal between them can be rewritten as

$$\begin{cases} \mathrm{X(z_t)} = \mathrm{CE}\beta_\mathrm{m}(\mathrm{z_t})\exp\left(-2\int_{z_b}^{z_t}\sigma_\mathrm{m}(\mathrm{z'})\mathrm{dz'}\right)\exp\left(-2\int_0^{z_b}\sigma(\mathrm{z'})\mathrm{dz'}\right) \\ \mathrm{X(z_t-1)} = \mathrm{CE}\beta_\mathrm{m}(\mathrm{z_t-1})\exp\left(-2\int_{z_b}^{z_t-1}\sigma_\mathrm{m}(\mathrm{z'})\mathrm{dz'}\right)\exp\left(-2\int_0^{z_b}\sigma(\mathrm{z'})\mathrm{dz'}\right) \\ \vdots \\ \mathrm{X(z_b+1)} = \mathrm{CE}\beta_\mathrm{m}(\mathrm{z_b+1})\exp\left(-2\int_{z_b}^{z_b+1}\sigma_\mathrm{m}(\mathrm{z'})\mathrm{dz'}\right)\exp\left(-2\int_0^{z_b}\sigma(\mathrm{z'})\mathrm{dz'}\right) \\ \mathrm{X(z_b)} = \mathrm{CE}\beta_\mathrm{m}(\mathrm{z_b})\exp\left(-2\int_{z_b}^{z_b}\sigma_\mathrm{m}(\mathrm{z'})\mathrm{dz'}\right)\exp\left(-2\int_0^{z_b}\sigma(\mathrm{z'})\mathrm{dz'}\right) \end{cases}. \tag{5}$$

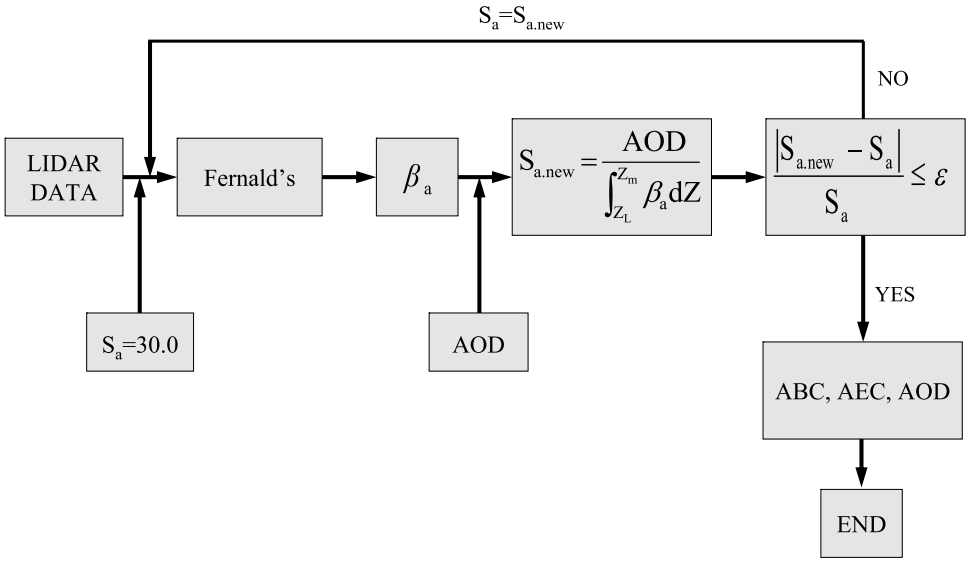

Figure 1. Flowchart of the retrieval algorithm used to obtain aerosol optical properties from lidar measurements in this study.

[16] Thus, we may conclude that linear relationships exist between the lidar range-corrected backscatter signal and air molecule optical properties in the selected region (from altitude Z_b to Z_t). If the slope of the straight line is denoted by K, then equation (5) changes as follow,

$$\begin{cases} X(z) = K\beta_m(z)\exp\left(-2\int_{z_b}^{z}\sigma_m(z')dz\right) \\ K = CE\exp\left(-2\int_{0}^{z_b}\sigma(z')dz'\right) \end{cases} (z_b \le z \le z_t). \quad (6)$$

In reality, it is impossible for the aforementioned region to be completely aerosol-free. Hence, a correction parameter δ for the backscatter signal from the aerosol is considered, and we have

$$\begin{cases} X(z) = K\beta_m(z)\exp\left(-2\int_{z_b}^{z}\sigma_m(z')dz'\right) + \delta \\ K = CE\exp\left(-2\int_{0}^{z_b}\sigma(z')dz'\right) \end{cases} (z_b \le z \le z_t). \quad (7)$$

The AOD integrated from ground to altitude z_b, can then be obtained from

$$AOD(z_b) = \int_0^{z_b}\sigma_a(z')dz' = \frac{1}{2}\ln\frac{CE}{K} - \int_0^{z_b}\sigma_m(z')dz'. \quad (8)$$

Accordingly, once the lidar system calibration constant C and molecular backscattering coefficient β_m or extinction coefficient σ_m is known, the AODs can be retrieved by the above method from lidar measurements without reference to the lidar ratio. β_m and σ_m can be determined from the best available meteorological sounding data or from appropriate standard atmospheres [*Fernald*, 1984] or from a co-located ground-based Atmospheric Emitted Radiance Interferometer (AERI) [*Feltz et al.*, 2003]. Estimating C from lidar measurements in the field has been discussed in some literatures [*Fernald et al.*, 1972; *Fernald*, 1984; *Powell et al.*, 2000; *Voss et al.*, 2001; *Reagan et al.*, 2002; *Liu et al.*, 2006], here we select a couple of clear days every month and estimate C from lidar observation according to equation (8) using AOD from co-located AERONET Sun photometer. Last, linear fit between the lidar range-corrected backscatter signal (Y) and air molecule optical properties (X) are made as $Y = KX + \delta$ to calculate the slope K of straight line. It deserves to be specially noted that the selection procedure of pre-identified atmospheric layer (from altitude Z_b to Z_t) for every profiles. To avoid identifying those pre-identified layers subjectively and empirically, we define the bottom Z_b of the layer depending on local past lidar observation results of seasonal average vertical profiles for every season and make the maximum observed altitude as the top Z_t; moreover, that Z_t should be higher by 2 km than Z_b is set in the calculating process to keep the error of K to a bare minimum. In the end, the aerosol backscattering coefficient (ABC), extinction coefficient (AEC), and layer-averaged lidar ratio can then be retrieved using these lidar-retrieved AODs as constraint [*Welton et al.*, 2000]. A flowchart of the retrieval algorithm is shown in Figure 1.

[17] Figure 1 indicates that the ABC could be obtained by assuming a constant lidar ratio (such as 30.0) via the method suggested by *Fernald* [1984]. The new lidar ratio is calculated from the relationship between ABC and the lidar-retrieved AOD to improve the estimate of S_a and is then used to calculate the new ABC again. The calculations use the lidar-retrieved AODs to be a constraint and continue until the difference between the new lidar ratio $S_{a.new}$ and S_a is less than a reasonable value (such as 5%). Hence, the final AEC can be calculated from the final ABC and the layer-averaged lidar ratio S_a. Finally, the final data products from the retrieval algorithm are ABC, AEC, layer-averaged lidar ratio, and

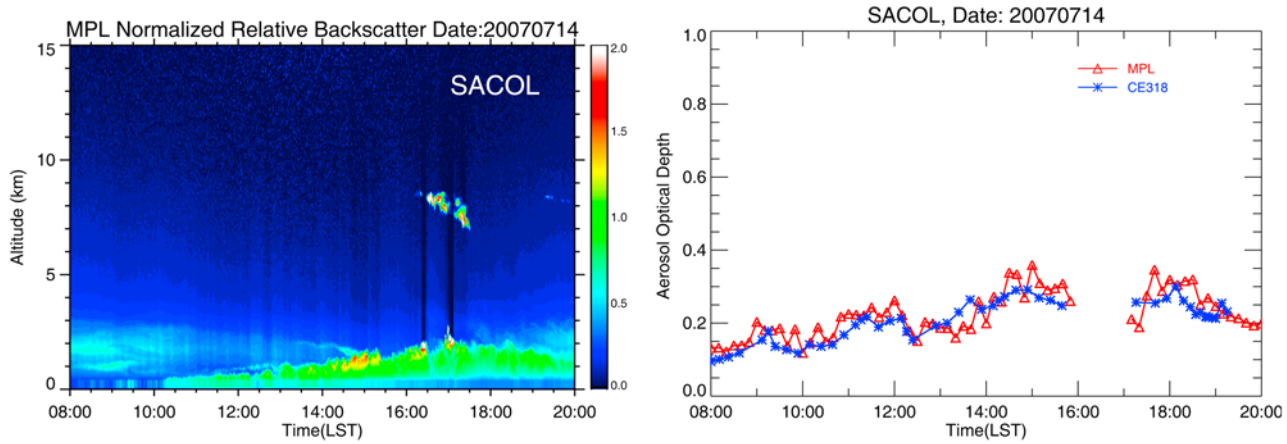

Figure 2. (left) MPL normalized relative backscatter at SACOL site and comparison between lidar-retrieved AODs and (right) corresponding results from AERONET CE318 measurements at 527 nm wavelength for 14 July 2007. The red line (triangles) represents lidar-obtained aerosol optical depths, and the blue line (asterisks) represents AODs obtained from AERONET CE318 measurements.

AOD. The effects of errors caused by the algorithm and the assumption of a constant S_a were tested with artificial lidar data by *Welton* [1998]. The advantage of the algorithm is that we do not need other independent instruments (e.g., Sun photometer or sky-radiometer) to provide AOD when retrieving ABC and AEC. It is an effective method for significantly reducing the errors caused by the lidar ratio when retrieving aerosol optical properties from Mie lidar measurements.

4. Validation

[18] In this section, lidar-retrieved AODs obtained from the above retrieval algorithm are validated using the corresponding AERONET Sun photometer (CE318) measurements.

[19] The time series for the MPL normalized relative backscatter at the SACOL site on 14 July 2007 is shown in Figure 2. The white color in Figure 2 represents a strong backscatter signal caused by the presence of clouds, and the green color represents atmospheric aerosols. The blue and black colors represent clean atmospheric conditions. The aerosol vertical structure remained very distinct all day. The strong lidar backscatter signal indicates a mass of local anthropogenic aerosols, as no dust aerosol was detected. The height of the aerosol layer rose continuously from 10 Local Standard Time (LST) and peaked at 17 LST. The aerosol layer was confined below 2 km, with only a small quantity of aerosol appearing at higher altitude. It is very exciting that the diurnal evolution and values of the AOD retrieved from the MPL at 527 nm are very close to the AERONET CE318 measurements for 14 July 2007.

[20] The AOD retrievals from the MPL for 17 and 19 September 2007 are also compared with the AERONET measurements, and the results for both dates are consistent (see Figures 3 and 4). These above results are strongly indicative of the reliability of lidar-retrieved AODs.

[21] However, more comparisons are needed to validate the superior reliability of the retrieval algorithm. AODs retrieved from long-term lidar measurements, taken at SACOL from April to October 2007, were compared to the corresponding AERONET CE318 measurements, and a scatterplot of the results is shown in Figure 5. One can observe that, except in

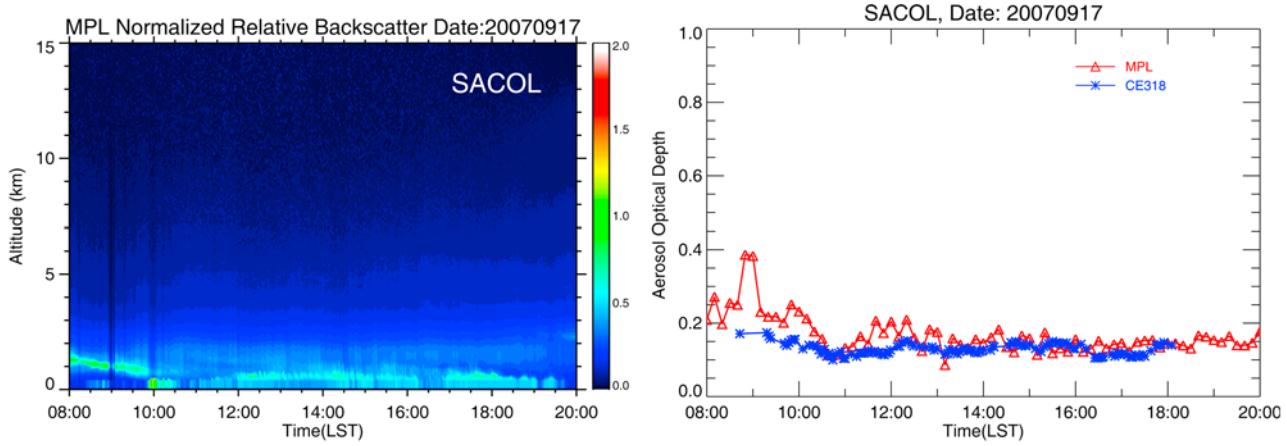

Figure 3. Same as Figure 2 but for 17 September 2007.

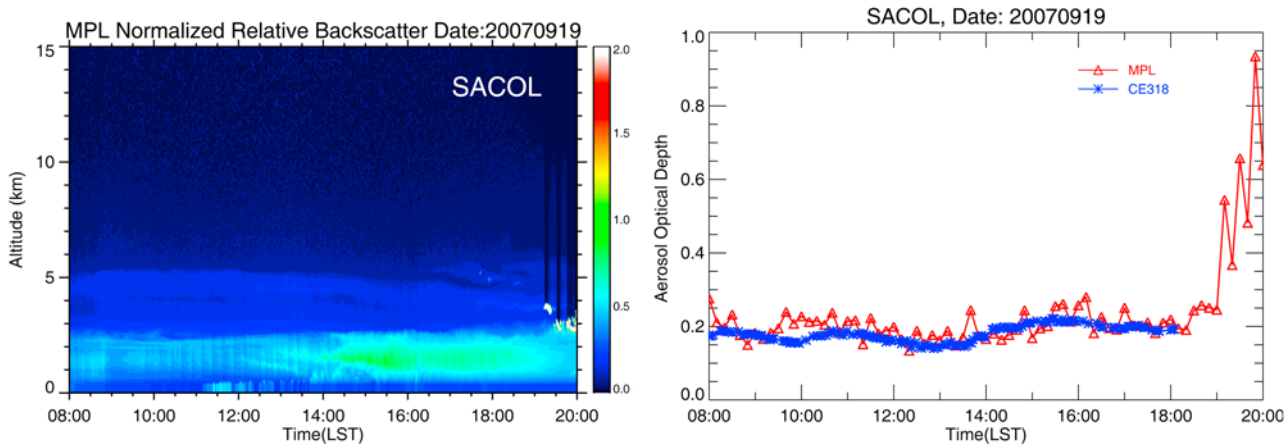

Figure 4. Same as Figure 2 but for 19 September 2007.

a few instances, most of the AOD retrievals from the MPL were consistent the AERONET measurements. The mean AODs for the CE318 and the MPL are 0.2414 and 0.2458, respectively, with a relative difference of 1.8209%. The root mean square difference (RMS) and correlation coefficient of the AODs retrieved from the MPL and the CE318 are 0.0603 and 0.8316, respectively. Moreover, the differences between the lidar-retrieved and CE318 AODs can be regarded (at least in part) as the result of the differing retrieval algorithms, as well as the aerosol spectral dependency. Further analysis will still be necessary to verify this behavior.

[22] The above results demonstrate that lidar-obtained AODs agree well with measurements obtained from the AERONET CE318. Therefore, the retrieval algorithm used to obtain AODs from the MPL is distinctly credible, and could be used in a wide range of lidar remote-sensing applications.

[23] More works should be done to further validate the algorithm. Obtaining AOD from lidar measurements using the algorithm still have existed other uncertainties, such as the uncertainties associated with the instrument calibration and the molecular optical properties. In the present paper, instrument calibration was estimated every month to ensure make the uncertainties caused by calibration as small as possible. Otherwise, the selection procedure of pre-identified atmospheric layer also should be more reasonable. In near future, this algorithm would be applied to retrieve the aerosol optical properties from NIES two-wavelength polarization lidar [*Sugimoto et al.*, 2002, 2006] and CIMEL single-wavelength micro lidar [*Pelon et al.*, 2008] measurements at SACOL. Although there are some uncertainties, it is a compromising solution without any better retrieval algorithm for Mie lidar measurements now. In this study, lidar-retrieved AODs have been proved to be reliable, namely, dust AEC retrieved from lidar measurements using the retrieval algorithm also is much more convictive than those results from assuming a constant S_a.

5. Case Study of Dust Storm

[24] Dust events occur frequently over East Asia in the spring, originating from the Taklimakan and Gobi deserts. Dust aerosols may be transported over long distances, to eastern China, Korea, and Japan [*Uematsu et al.*, 2002; *Zhang et al.*, 2003; *Liu et al.*, 2008b], and even to the Pacific Ocean and North America [*Arimoto et al.*, 1996; *Takemura et al.*, 2002; *Uno et al.*, 2001; *Huang et al.*, 2008a]. On 2 May 2008, a major dust storm occurred over Northwest China and was considered to be one of the worst dust events in 2008. Because Aura/OMI is especially useful for monitoring the dust storms that commonly occur over desert or semi-arid regions [*Li*, 1998, 2004], AI from OMI measurements were employed to identify dust aerosols and describe the influencing intensity and transport path of the dust in this study.

[25] AI from OMI observations over Northwest China from 1 to 3 May 2008 are shown in Figure 6. On 1 May 2008, AI was comparatively low due to the lack of absorbing aerosols over Northwest China. However, AI increased as the dust storm approached, and they peaked on 2 May 2008. After the dust storm moved out of the study areas, the AI decreased, but they were still larger on 3 May than on 1 May because of the residual dust aerosol. Furthermore, a west-to-east transport of dust aerosols was clearly detected from the OMI measurements.

[26] To better study the characteristics of formation mechanism of the dust storm, synoptic analysis is very valuable to

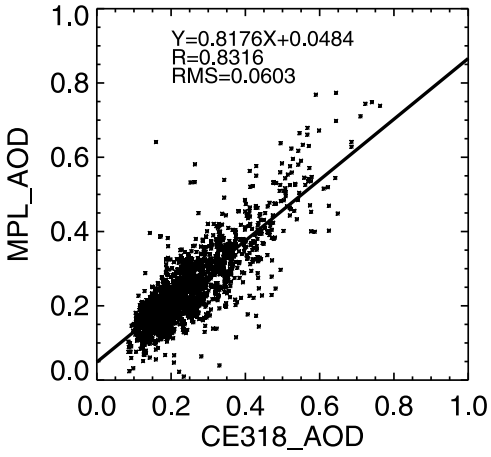

Figure 5. Scatterplot comparing lidar-retrieved AODs and corresponding results from the CE318, both at 527 nm wavelength, for April to October 2007 at SACOL.

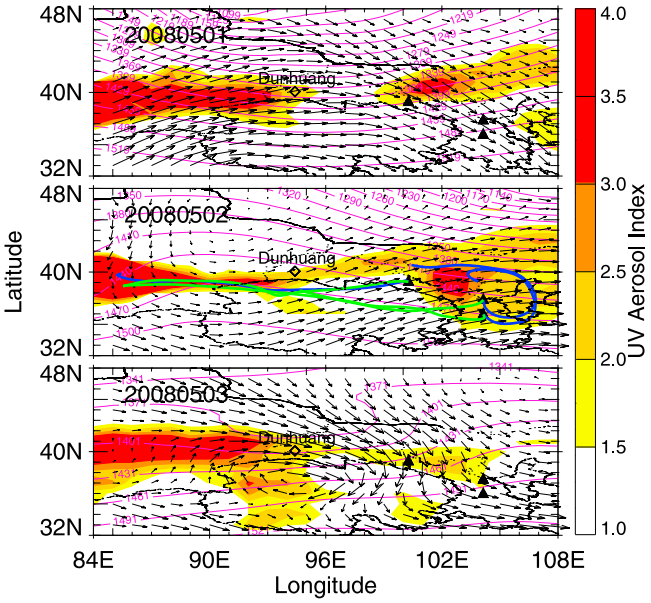

Figure 6. UV AI from OMI observations, 850 hPa geometric height fields (magenta line) and wind fields (black arrows) from NCEP reanalysis data over Northwest China for (top) 1 (middle) 2 and (bottom) 3 May 2008. The blue and green thick lines represent the 36-h backward trajectory for each site at 15 LST for 1 km and 2 km AGL, respectively. The time of synoptic charts for every day is 14 LST. The black triangles indicate the locations of the SACOL (35.946N, 104.137E), Jingtai (37.332N, 104.139E), and Zhangye (39.078N, 100.272E) sites.

interpret the dust events. Some recent studies also use synoptic charts help to demonstrate dust events and obtain much valuable results. *Sun et al.* [2001] claimed that dust storm genesis is related to cold air outbreaks by cyclones or frontal systems. *Gao et al.* [2002] also pointed out that the generating area of the dust storms is consistent with the tracks of synoptic-scale disturbances. *Aoki et al.* [2005] found dust storms in the Tarim basin of Northwest China are generated by a mesoscale cold wind system induced by a synoptic scale cold air mass behind a cold front. In present study, the synoptic charts of 850 hPa geometric height field and wind field over Northwest China at 14 LST for 1–3 May 2008 from NCEP/NCAR reanalysis data [*Kalnay et al.*, 1996] are used to describe the dust storm as also shown in Figure 6. The colder Siberia air mass from Gobi desert goes around the eastern side of the Taklimakan desert and then turns eastward and advances across Tenggeli desert. Strong geometric height gradients lead too much stronger wind from west to east. A low pressure which located around Mongolian plateau also leads to the dust storm. These results is similar with the results by *Liu et al.* [2004], which pointed out the colder Siberia air mass, stronger and longer troughs or cyclones in and around Mongolia, and stronger mid- and lower-level westerly winds around the China-Mongolia border are key features leading to more major dust storms in western China-Mongolia in the spring.

[27] At the same time, a backward trajectory analysis was conducted to find the source region of the dust aerosols (as shown in Figure 6). The NOAA/Air Resources Laboratory HYbrid Single-Particle Lagrangian Integrated Trajectory (HYSPLIT) model (R. R. Draxler and G. D. Rolph, HYSPLIT (Hybrid Single-Particle Lagrangian Integrated Trajectory) Model, 2003, access via NOAA ARL READY Web site, http://www.arl.noaa.gov/ready/hysplit4.html) was used to calculate the 36-h backward trajectories of the air masses, employing the Global Data Assimilation System (GDAS) meteorological data set of the NCEP as input. Three arrival points were selected in the altitude range of 1000 m (blue line) to 2000 m (red line) according to the location of the dust aerosol layers. If an air mass originates in a dust source region, it can be hypothetically labeled as a dust aerosol. At 15 LST, at an altitude of 1000 m, the air masses of Jingtai and SACOL flowed from the Tenggeli desert, while the Zhangye air masses came from the Taklimakan desert. At the same time, at an altitude of 2000 m, the air masses of all three sites flowed from the Taklimakan desert. According to the back trajectory analysis, dust-laden air masses were predominant. The dust event originated in the Taklimakan Desert on 2 May 2008 and was transported to the Zhangye, SACOL, and Jingtai sites. Some of the dust aerosols also originated in the Gobi and Tenggeli deserts.

[28] The dust event was simultaneously observed by the space-borne lidar CALIPSO when it passed over Northwest China on 2 May 2008 (as shown in Figure 7). Figure 7 (top) indicates that high-concentration aerosol layers were observed, which produced a strong backscatter lidar signal over Northwest China (the selected area) in the morning (at about 03:50 LST). That the aerosol layer was a dust layer can be inferred from the high depolarization ratio (larger than 0.3), which indicates non-spheroid coverage (typical of dust aerosols) [*Hu et al.*, 2007], as shown as Figure 7 (middle). Moreover, the CALIPSO measurements show that the altitude of the dust aerosol layer was approximately 2 km above ground level, and the area of influence of the dust event was very wide (roughly 550 km).

[29] Early in the morning of 2 May, the dust event was observed via vertical MPL measurements taken at Zhangye, as shown in Figure 8. The progressive fine changes in the dust event are displayed in a time series of the normalized relative backscatter. Traces of the dust aerosol structure were observed in the region below 3 km above ground level, at the bottom of the troposphere. This structure grew steadily, and the top of the dust layer remained at an altitude of approximately 3 km during the dust storm but was at an altitude of about 2 km during the early morning hours. By 14:30 LST, 10 h after the dust layer was first observed, the vertical extension of the dust layer had thickened to about 3.5 km. The strongest return signal for the dust layer observed by the Zhangye MPL measurements occurred at around 15 LST. After this time, the layer strength began to weaken. Cloud formation began at 14 LST, and it started to rain at 17:40 LST. A possible explanation for this occurrence is that particles in the dust aerosol acted as cloud condensation nuclei (CCN), causing the rain and also furnishing evidence of an aerosol indirect effect. In addition to the lidar measurements at Zhangye, the vertical structure of the dust event was observed at Jingtai and SACOL (Figure 8). Unfortunately, the MPL at Jingtai was not functioning normally before 11:30 LST due to an unstable power supply. However, floating dust was observed by other instruments (such as the Sun photometer,

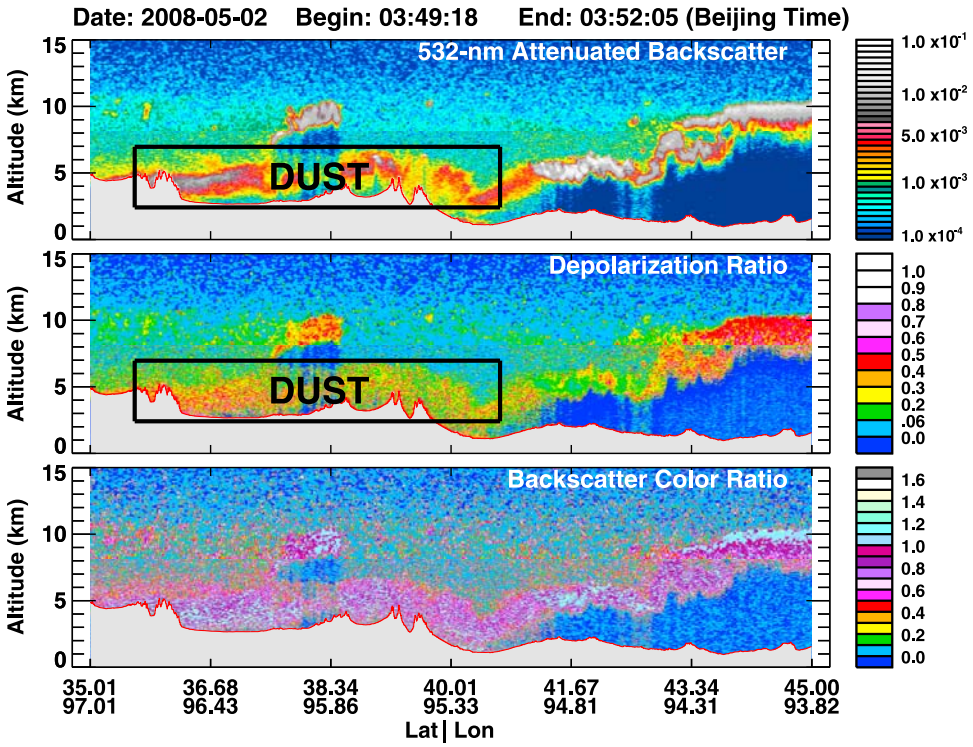

Figure 7. Atmospheric vertical structure from space-borne CALIPSO measurement: (top) 532 nm total attenuated backscatter, (middle) depolarization ratio and (bottom) backscatter color ratio over Northwest China for 2 May 2008.

Andersen sampler, etc.) and was also recorded in the daily notebook by personnel at the site. In contrast to the measurements at Zhangye, the dust layer was confined to below 2 km at Jingtai and below 1.5 km at the SACOL site. The strongest dust intensity was observed at Zhangye, followed by the Jingtai site, and finally SACOL, corresponding to increasing distance from the desert source. Because the thick dust layer moved out of the experimental region, and moisture from the subsequent precipitation quickly reduced the aerosol concentration, the dust intensity weakened rapidly during the early evening.

[30] The vertical distribution of the aerosol extinction coefficient was retrieved from MPL normalized relative backscatter using the aforementioned algorithm. Figure 9 shows the vertical distributions of the MPL aerosol extinction coefficient at Zhangye, Jingtai, and SACOL, respectively. The solid and dashed lines represent the vertical distribution of the aerosol extinction coefficient in the morning (before the arrival of the dust event) and in the afternoon (at the strongest of the dust event), respectively. The three sites had some common aerosol vertical profile characteristics, such as an aerosol extinction coefficient that decreased with height and peaked at a certain altitude. However, the differences between them are too great to be disregarded. The aerosol heights differed significantly at the three sites. The altitude at which the aerosol extinction coefficient peaked was different for different times and sites. At the Zhangye site, obvious multilayers were observed, whereas this phenomenon did not occur at the other two sites. One reason for this may be that the Zhangye site is closest to the desert source region, and pure dust aerosols do not mix well. Better mixing occurs when the dust aerosols are adulterated with other kinds of aerosol over long distances, which may explain why mixed aerosols were observed at Jingtai and SACOL. Of course, both the physical and chemical properties of the dust aerosol are greatly changed in transport.

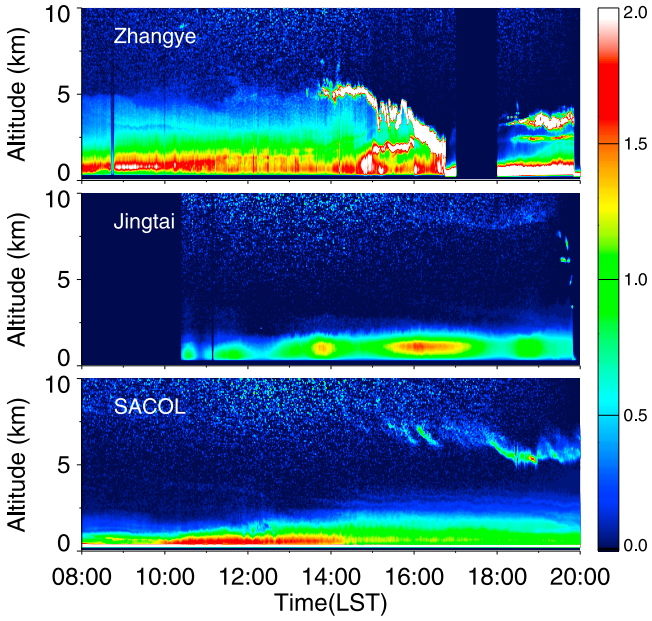

Figure 8. MPL normalized relative backscatter at the Zhangye, Jingtai, and SACOL sites for 2 May 2008.

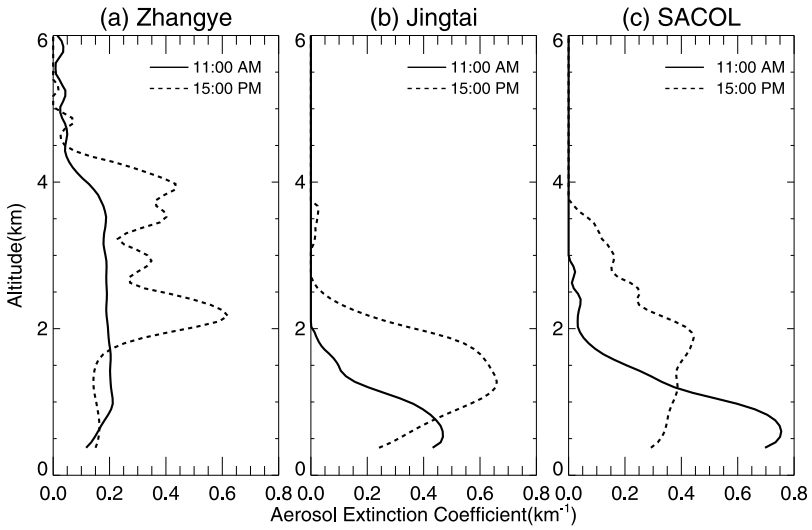

Figure 9. Vertical distribution of MPL aerosol extinction coefficient at the (a) Zhangye, (b) Jingtai, and (c) SACOL sites for 2 May 2008.

[31] Figure 10 displays the diurnal cycle of dust aerosol optical properties for the duration of the dust event. At Zhangye site, the AOD was under 0.5 in the morning (when the dust storm was approaching) but increased rapidly and peaked at 0.8 around 17:00 LST. At the Jingtai site, the AOD was also under 0.5 (and less than at Zhangye) in the morning and then increased steadily to a peak that occurred around 17:00 LST. The AOD at SACOL exhibited the same behavior but was less than other two sites at the strongest of the dust event.

6. Characteristics of Aerosol Vertical Profiles

[32] It is important to investigate the seasonal average vertical profiles of aerosol optical properties over Northwest China, especially in the spring when dust storms occur frequently.

[33] Figure 11 shows the daily changes of the monthly average aerosol vertical structure at the Zhangye, Jingtai, and SACOL sites in the spring (from March to May 2008).

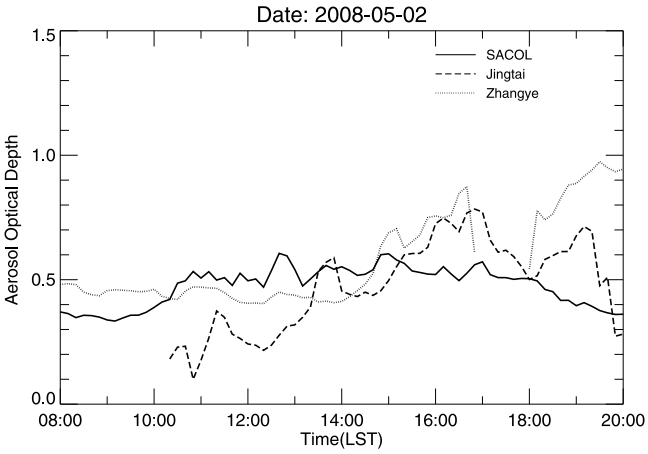

Figure 10. Diurnal cycle of AODs for duration of the dust event.

Clouds were screened using the wavelet method to detect discontinuities in the lidar signal as the base, the top and the peak backscatter of individual cloud layers and line fit [*Mallat and Hwang*, 1992; *Brooks*, 2003; *Wang and Sassen*, 2001; *Morille et al.*, 2007]. The results show that aerosol concentrations are much higher in the afternoon than in the morning. At Zhangye, a higher concentration of aerosol is observed in April than in May. At Jingtai, the highest concentration of aerosol occurs in May and at SACOL in April. A notable result is that the aerosol masses at all three sites are comparable, especially in April. One reason for this is

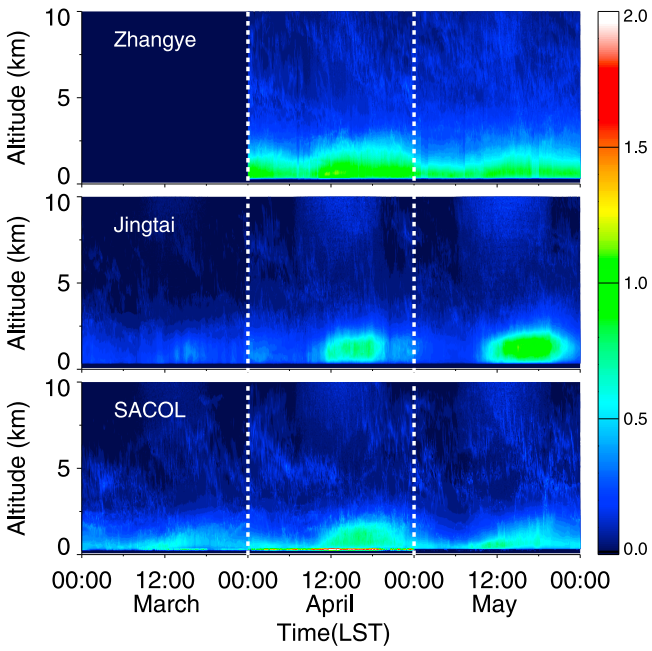

Figure 11. Daily changes of monthly average aerosol vertical structure at the Zhangye, Jingtai, and SACOL sites in the spring (from March to May 2008).

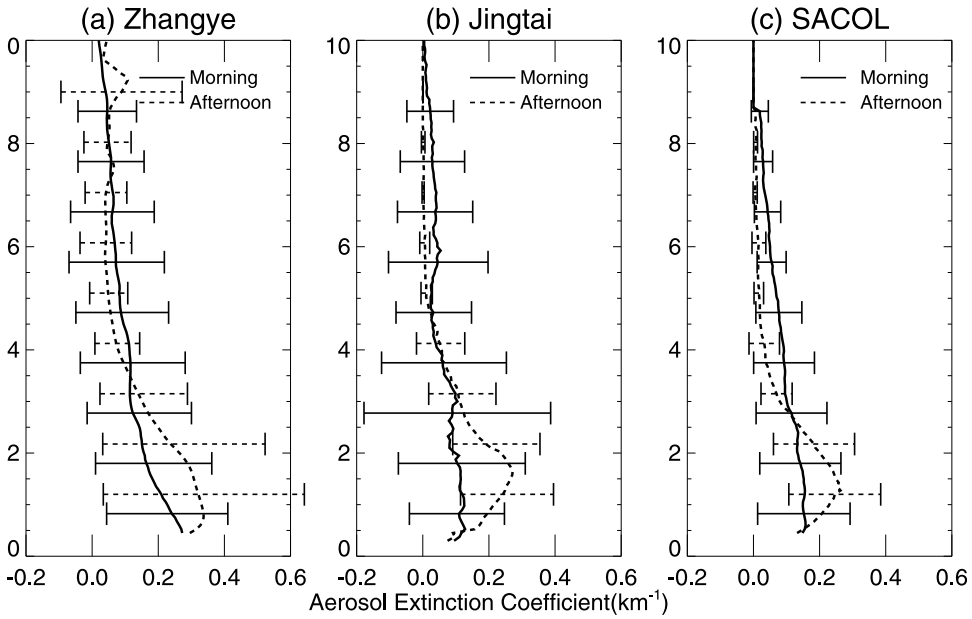

Figure 12. Seasonal average vertical profiles of the MPL aerosol extinction coefficients at the (a) Zhangye, (b) Jingtai, and (c) SACOL sites for March to May 2008. Error bars are standard deviations computed from the vertical bins of each profile.

that dust aerosols are transported over long distances and typically pass over all three sites. It seems inconceivable that relatively little aerosol is present at Jingtai in March, as dust events are fewer in March than in April, and the air quality in March is comparatively good. At any rate, the analysis results indicate that aerosol mass is strongly related to the occurrence of dust events.

[34] Figure 12 shows the seasonal average vertical profiles of the MPL aerosol extinction coefficients at the Zhangye, Jingtai, and SACOL sites from March to May 2008. The error bars are standard deviations computed from the vertical bins of each profile. In the morning, the aerosol extinction coefficient at each site is substantial (the lowest being at Jingtai), and most of the aerosols stay at the bottom of the troposphere. In the afternoon, peaks occur at 1.5 km and 1.3 km for Jingtai and SACOL, respectively. Some aerosols are suspended at higher altitudes at the Zhangye site, with a significantly lesser amount at SACOL and hardly any at Jingtai. This is because more aerosols tend to remain at high altitudes in the vicinity of a dust source. The error bars may show the fluctuation of variance and indicate the stabilization of the aerosol vertical structure at each altitude. We can see that the error bars for Zhangye and Jingtai are higher than those for SACOL in the spring. The reason for this is that the Zhangye and Jingtai sites are influenced by several aerosol sources, such as the Taklimakan, Gobi, Badanjilin, and Tenggeli deserts. Although the SACOL site is located in the only path of long-range dust aerosol transport, the aerosol vertical structure at SACOL is much more stable.

7. Summary and Conclusion

[35] The 2008 China-U.S. joint dust field experiment, which aims to estimate the effect of dust on radiative forcing and its associated climatic impacts, was conducted during the dust-intensive observation period from March to June of 2008 over the Loess Plateau of Northwest China. Dust aerosol vertical profiles and long-range transport of dust storm were measured with three MPL-net MPL systems as well as other ground-based instruments and space-borne remote sensing techniques.

[36] In this study, to ensure the effectiveness of the retrieval results, an effective algorithm was introduced for retrieving aerosol optical properties and vertical profiles from Mie lidar measurements. The advantage of this algorithm is that AOD retrieval from lidar measurements can be accomplished without the use of the so-called lidar ratio for the corresponding quantities obtained from the AERONET CE318. Moreover, errors in retrieving other optical properties are apparently reduced by using the measured AOD as a constraint. Dust aerosol vertical profiles are derived successfully from the three MPL Lidar systems using this algorithm. A dust storm that affected a large part of Northwest China on 2 May, 2008 was studied in detail using measurements obtained from the three ground-based lidar systems, satellite-borne instruments. The Aura/OMI instruments, NOAA/Air Resources Laboratory HYSPLIT model, and space-borne lidar CALIPSO were also used to analyze the sources of the dust storm. The dust event originated in the Taklimakan, Gobi, and Tenggeli deserts, and distinct aerosol vertical structures occurred at each site. Synoptic charts from NCEP reanalysis data help to demonstrate dust events and show that the colder Siberia air mass and stronger and longer cyclones around Mongolia are key features leading to the dust storm.

[37] Finally, characteristics of the aerosol vertical structure over Northwest China in the spring were also investigated. Aerosol mass is strongly related to the occurrence of dust events. Comparing the three sites, the aerosol intensity was highest at Zhangye and lowest at SACOL. Nearer the dust source, more aerosol remains at high altitudes. The aerosol

vertical structures at SACOL are much more stable than those at the other sites, as they are influenced less by aerosol sources. In contrast, the structures vary sharply at Zhangye.

[38] **Acknowledgments.** This work was funded by the National Science Foundation of China under grants 40725015 and 40633017. The cooperative experiment was conducted by Lanzhou University, University of Maryland (USA), and Institute of Atmospheric Physics (CAS, China). The authors would like to thank all the people who worked for the 2008 China-U.S. joint dust field experiment so as to get such high-quality data sets. We are grateful to R. Coulter of the Argonne National Lab for loaning a MPL used in this study. We also thank the OMI and CALIPSO team for providing satellite data sets. The authors gratefully acknowledge the NOAA Air Resources Laboratory (ARL) for the provision of the HYSPLIT transport and dispersion model and/or READY website (http://www.arl.noaa.gov/ready.html) used in this publication.

References

Ackermann, J. (1997), Two-wavelength lidar inversion algorithm for a two-component atmosphere, *Appl. Opt.*, *36*, 5134–5143, doi:10.1364/AO.36.005134.

Ångström, A. (1929), On the atmospheric transmission of Sun radiation and on dust in the air, *Geogr. Ann.*, *11*, 156–166, doi:10.2307/519399.

Ångström, A. (1930), On the atmospheric transmission of Sun radiation II, *Geogr. Ann.*, *12*, 130–159, doi:10.2307/519561.

Aoki, I., Y. Kurosaki, R. Osada, T. Sato, and F. Kimura (2005), Dust storms generated by mesoscale cold fronts in the Tarim Basin, northwest China, *Geophys. Res. Lett.*, *32*, L06807, doi:10.1029/2004GL021776.

Arimoto, R., R. A. Duce, D. L. Savoie, J. M. Prospero, R. Talbot, J. D. Cullen, U. Tomza, N. F. Lewis, and B. J. Ray (1996), Relationships among aerosol constituents from Asia and the North Pacific during PEM-West A, *J. Geophys. Res.*, *101*(D1), 2011–2023, doi:10.1029/95JD01071.

Brooks, I. M. (2003), Finding boundary layer top: Application of a wavelet covariance transform to lidar backscatter profiles, *J. Atmos. Oceanic Technol.*, *20*, 1092–1105, doi:10.1175/1520-0426(2003)020<1092:FBLTAO>2.0.CO;2.

Cachorro, V. E., A. M. de Frutos, and J. L. Casanova (1987), Determination of the Ångström turbidity parameters, *Appl. Opt.*, *26*, 3069–3076, doi:10.1364/AO.26.003069.

Campbell, J. R., et al. (2002), Full-time, eye-safe cloud and aerosol lidar observation at Atmospheric Radiation Measurement program sites: Instruments and data processing, *J. Atmos. Oceanic Technol.*, *19*, 431–442, doi:10.1175/1520-0426(2002)019<0431:FTESCA>2.0.CO;2.

Carlos, T., V. Cachorro, A. Berjon, M. Sorribas, R. Vergaz, A. Defrutos, and M. Anton (2006), Aerosol optical depth at ALOMAR Observatory (Andøya, Norway) in summer 2002 and 2003, *Tellus, Ser. B*, *58*, 218–228.

Carlson, T. N., and S. G. Benjamin (1980), Radiative heating rates for Saharan dust, *J. Atmos. Sci.*, *37*(1), 193–213, doi:10.1175/1520-0469(1980)037<0193:RHRFSD>2.0.CO;2.

Chand, D., T. L. Anderson, R. Wood, R. J. Charlson, Y. Hu, Z. Liu, and M. Vaughan (2008), Quantifying above-cloud aerosol using spaceborne lidar for improved understanding of cloudy-sky direct climate forcing, *J. Geophys. Res.*, *113*, D13206, doi:10.1029/2007JD009433.

Claquin, T., et al. (1998), Uncertainties in assessing radiative forcing by mineral dust, *Tellus, Ser. B*, *50*, 491–505.

Claquin, T., M. Schulz, and Y. J. Balkanski (1999), Modeling the mineralogy of atmospheric dust sources, *J. Geophys. Res.*, *104*(D18), 22,243–22,256, doi:10.1029/1999JD900416.

Eck, T. F., B. N. Holben, J. S. Reid, O. Dubovik, A. Smirnov, N. T. O'Neill, I. Slutsker, and S. Kinne (1999), Wavelength dependence of the optical depth of biomass burning, urban, and desert dust aerosol, *J. Geophys. Res.*, *104*(D24), 31,333–31,349, doi:10.1029/1999JD900923.

Esselborn, M., M. Wirth, A. Fix, M. Tesche, and G. Ehret (2008), Airborne high spectral resolution lidar for measuring aerosol extinction and backscatter coefficients, *Appl. Opt.*, *47*, 346–358, doi:10.1364/AO.47.000346.

Feltz, W. F., H. B. Howell, R. O. Knuteson, H. M. Woolf, and H. E. Revercomb (2003), Near continuous profiling of temperature, moisture, and atmospheric stability using the Atmospheric Emitted Radiance Interferometer (AERI), *J. Appl. Meteorol.*, *42*, 584–597, doi:10.1175/1520-0450(2003)042<0584:NPOTMA>2.0.CO;2.

Fernald, F. G. (1984), Analysis of atmospheric lidar observations: Some comments, *Appl. Opt.*, *23*, 652–653, doi:10.1364/AO.23.000652.

Fernald, F. G., B. M. Herman, and J. A. Reagan (1972), Determination of aerosol height distributions by lidar, *J. Appl. Meteorol.*, *11*, 482–489, doi:10.1175/1520-0450(1972)011<0482:DOAHDB>2.0.CO;2.

Forster, P., et al. (2007), Changes in atmospheric constituents and in radiative forcing, in *Climate Change 2007: The Physical Science Basis, Working Group I to the Fourth Assessment Report of the Intergovernmental Panel on Climate Change*, edited by S. Solomon et al., pp. 129–234, Cambridge Univ. Press, Cambridge, U. K.

Franke, K., A. Ansmann, D. Müller, D. Althausen, F. Wagner, and R. Scheele (2001), One-year observations of particle lidar ratio over the tropical Indian Ocean with Raman lidar, *Geophys. Res. Lett.*, *28*, 4559–4562, doi:10.1029/2001GL013671.

Gao, X., S. Yabuki, Z. Qu, and Z. Qian (2002), Some characteristics of dust storm in northwest China, *J. Arid Land Stud.*, *11*(4), 235–243.

Guan, X., J. Huang, N. Guo, J. Bi, and G. Wang (2009), Variability of soil moisture and its relationship with surface albedo and soil thermal parameters over the Loess Plateau, *Adv. Atmos. Sci.*, *26*(4), 692–700, doi:10.1007/s00376-009-8198-0.

He, Q., and J. Mao (2004), Micro-Pulse Lidar and its applications (in Chinese), *Meteorol. Sci. Technol.*, *32*(4), 219–224.

Holben, B. N., et al. (1998), AERONET—A federated instrument network and data archive for aerosol characterization, *Remote Sens. Environ.*, *66*, 1–16, doi:10.1016/S0034-4257(98)00031-5.

Hu, Y., et al. (2007), The depolarization−attenuated backscatter relation: CALIPSO lidar measurements vs. theory, *Opt. Express*, *15*, 5327–5332, doi:10.1364/OE.15.005327.

Hua, D., M. Uchida, and T. Kobayashi (2004), UV high-spectral-resolution Rayleigh-Mie lidar with dual-pass Fabry-Perot etalon for measuring atmospheric temperature profiles of the troposphere, *Opt. Lett.*, *29*(10), 1063–1065, doi:10.1364/OL.29.001063.

Huang, J., P. Minnis, Y. Yi, Q. Tang, X. Wang, Y. Hu, Z. Liu, K. Ayers, C. Trepte, and D. Winker (2007), Summer dust aerosols detected from CALIPSO over the Tibetan Plateau, *Geophys. Res. Lett.*, *34*, L18805, doi:10.1029/2007GL029938.

Huang, J., P. Minnis, B. Chen, Z. Huang, Z. Liu, Q. Zhao, Y. Yi, and J. K. Ayers (2008a), Long-range transport and vertical structure of Asian dust from CALIPSO and surface measurements during PACDEX, *J. Geophys. Res.*, *113*, D23212, doi:10.1029/2008JD010620.

Huang, J., et al. (2008b), An overview of the semi-arid climate and environment research observatory over the Loess Plateau, *Adv. Atmos. Sci.*, *25*(6), 906–921, doi:10.1007/s00376-008-0906-7.

Huang, J., Z. Huang, J. Bi, W. Zhang, and L. Zhang (2008c), Micro-pulse lidar measurements of aerosol vertical structure over the Loess Plateau, *Atmos. Oceanic Sci. Lett.*, *1*, 8–11.

Huang, J., Q. Fu, J. Su, Q. Tang, P. Minnis, Y. Hu, Y. Yi, and Q. Zhao (2009), Taklimakan dust aerosol radiative heating derived from CALIPSO observations using the Fu-Liou radiation model with CERES constraints, *Atmos. Chem. Phys.*, *9*, 4011–4021, doi:10.5194/acp-9-4011-2009.

Kalnay, E., et al. (1996), The NCEP/NCAR 40-year reanalysis project, *Bull. Am. Meteorol. Soc.*, *77*, 437–471, doi:10.1175/1520-0477(1996)077<0437:TNYRP>2.0.CO;2.

Klett, J. D. (1981), Stable analytical inversion solution for processing lidar returns, *Appl. Opt.*, *20*, 211–220, doi:10.1364/AO.20.000211.

Kohl, R. H. (1978), Discussion of the interpretation problem encountered in single-wavelength lidar transmissometers, *J. Appl. Meteorol.*, *17*, 1034–1038, doi:10.1175/1520-0450(1978)017<1034:DOTIPE>2.0.CO;2.

Kovalev, V. A. (1993), Lidar measurement of the vertical aerosol extinction profiles with range-dependent backscatter-to extinction ratios, *Appl. Opt.*, *32*, 6053–6065, doi:10.1364/AO.32.006053.

Li, Z. (1998), Influence of absorbing aerosols on the inference of solar surface radiation budget and cloud absorption, *J. Clim.*, *11*, 5–17, doi:10.1175/1520-0442(1998)011<0005:IOAAOT>2.0.CO;2.

Li, Z. (2004), Aerosol and climate: A perspective over East Asia, in *Observation, Theory and Modeling of Atmospheric Variability*, edited by X. Zhu et al., pp. 501–525, World Sci., Singapore.

Li, Z., et al. (2007), Preface to special section on East Asian Studies of Tropospheric Aerosols: An International Regional Experiment (EAST-AIRE), *J. Geophys. Res.*, *112*, D22S00, doi:10.1029/2007JD008853.

Liao, H., and J. H. Seinfeld (1998), Radiative forcing by mineral dust aerosols: Sensitivity to key variables, *J. Geophys. Res.*, *103*(D24), 31,637–31,645, doi:10.1029/1998JD200036.

Liu, C., Z. Qian, M. Wu, M. Song, and J. Liu (2004), A composite study of the synoptic differences between major and minor dust storm springs over the China-Mongolia Areas, *Terr. Atmos. Oceanic Sci.*, *15*(5), 999–1018.

Liu, Z., Y. Hu, M. Vaughan, J. Reagan, C. Hostetler, D. Winker, W. Hunt, K. Powell, and C. Trepte (2006), Validation of CALIPSO Lidar (CALIOP) calibration, paper presented at 23rd International Laser Radar Conference, INDECO, Inc., Nara, Japan.

Liu, Z., et al. (2008a), CALIPSO lidar observations of optical properties of Saharan dust: A case study of long-range transport, *J. Geophys. Res.*, *113*, D07207, doi:10.1029/2007JD008878.

Liu, Z., et al. (2008b), Airborne dust distributions over the Tibetan Plateau and surrounding areas derived from the first year of CALIPSO lidar observations, *Atmos. Chem. Phys.*, *8*, 5045–5060, doi:10.5194/acp-8-5045-2008.

Lü, D., et al. (1977), Vertical distribution of the extinction coefficient of lower atmosphere explored by lidar, *Chin. J. Atmos. Sci.*, *1*(3), 199–205.

Mallat, S. G., and W. L. Hwang (1992), Singularity detection and processing with wavelets, *IEEE Trans. Inf. Theory*, *38*, 617–643, doi:10.1109/18.119727.

Measures, R. M. (1984), *Laser Remote Sensing: Fundamentals and Applications*, 510 pp., John Wiley, Hoboken, N. J.

Meloni, D., A. D. Sarra, T. D. Iotio, and G. Fiocco (2005), Influence of the vertical profile of Saharan dust on the visible direct radiative forcing, *J. Quant. Spectrosc. Radiat. Transfer*, *93*, 397–413, doi:10.1016/j.jqsrt.2004.08.035.

Minnis, P., and S. K. Cox (1978), Magnitude of the radiative effects of the Sahara dust layer, *Atmos. Sci. Pap. 283*, 111 pp., Colo. State Univ., Ft. Collins.

Morille, Y., M. Haeffelin, P. Drobinski, and J. Pelon (2007), STRAT: An automated algorithm to retrieve the vertical structure of the atmosphere from single-channel lidar data, *J. Atmos. Oceanic Technol.*, *24*, 761–775, doi:10.1175/JTECH2008.1.

Pelon, J., M. Mallet, A. Mariscal, P. Goloub, D. Tanré, D. Bou Karam, C. Flamant, J. Haywood, B. Pospichal, and S. Victori (2008), Microlidar observations of biomass burning aerosol over Djougou (Benin) during African Monsoon Multidisciplinary Analysis Special Observation Period 0: Dust and Biomass-Burning Experiment, *J. Geophys. Res.*, *113*, D00C18, doi:10.1029/2008JD009976.

Potter, J. F. (1987), Two-frequency lidar inversion technique, *Appl. Opt.*, *26*, 1250–1256, doi:10.1364/AO.26.001250.

Powell, D. M., et al. (2000), ACE-2 multiple angle micro-pulse lidar observations from Las Galletas, Tenerife, Canary Islands, *Tellus, Ser. B*, *52*, 652–661.

Qiu, J., et al. (2003), Lidar measurements of cloud and aerosol in the upper troposphere in Beijing (in Chinese), *Chin. J. Atmos. Sci.*, *27*, 1–7.

Ramanathan, V., P. J. Crutzen, J. T. Kiehl, and D. Rosenfeld (2001), Aerosols, climate, and the hydrological cycle, *Science*, *294*, 2119–2124, doi:10.1126/science.1064034.

Reagan, J. A., M. V. Apte, A. Ben-David, and B. M. Herman (1988), Assessment of aerosol extinction to back-scatter ratio measurements made at 694.3 nm in Tucson, Arizona, *Aerosol Sci. Technol.*, *8*, 215–226, doi:10.1080/02786828808959184.

Reagan, J. A., X. Wang, and M. T. Osborn (2002), Spaceborne lidar calibration from cirrus and molecular backscatter returns, *IEEE Trans. Geosci. Remote Sens.*, *40*, 2285–2290, doi:10.1109/TGRS.2002.802464.

Roy, G., G. Vallee, and M. Jean (1993), Lidar-inversion technique based on total integrated backscatter calibrated curves, *Appl. Opt.*, *32*, 6754–6763, doi:10.1364/AO.32.006754.

Satheesh, S. K., and V. Ramanathan (2000), Large difference in tropical aerosol forcing at the top of the atmosphere and Earth's surface, *Nature*, *405*, 60–63, doi:10.1038/35011039.

Sokolik, I. N., and O. B. Toon (1996), Direct radiative forcing by anthropogenic airborne mineral aerosols, *Nature*, *381*, 681–683, doi:10.1038/381681a0.

Spinhirne, J. D. (1993), Micro Pulse Lidar, *IEEE Trans. Geosci. Remote Sens.*, *31*, 48–55, doi:10.1109/36.210443.

Stephens, G. L., R. J. Engelen, M. Vaughan, and T. L. Anderson (2001), Toward retrieving properties of the tenuous atmosphere using space-based lidar measurements, *J. Geophys. Res.*, *106*(D22), 28,143–28,157, doi:10.1029/2001JD000632.

Sugimoto, N., I. Matsui, A. Shimizu, I. Uno, K. Asai, T. Endoh, and T. Nakajima (2002), Observation of dust and anthropogenic aerosol plumes in the northwest Pacific with a two-wavelength polarization lidar on board the research vessel Mirai, *Geophys. Res. Lett.*, *29*(19), 1901, doi:10.1029/2002GL015112.

Sugimoto, N., et al. (2006), Network observations of Asian dust and air pollution aerosols using two-wavelength polarization lidars, paper presented at 23rd International Laser Radar Conference, INDECO, Inc., Nara, Japan.

Sun, J., M. Zhang, and T. S. Liu (2001), Spatial and temporal characteristics of dust storms in China and its surrounding regions, 1960–1999: Relations to source area and climate, *J. Geophys. Res.*, *106*(D10), 10,325–10,333, doi:10.1029/2000JD900665.

Takemura, T., I. Uno, T. Nakajima, A. Higurashi, and I. Sano (2002), Modeling study of long-range transport of Asian dust and anthropogenic aerosols from East Asia, *Geophys. Res. Lett.*, *29*(24), 2158, doi:10.1029/2002GL016251.

Torres, O., P. K. Bhartia, J. R. Herman, and Z. Ahmad (1998), Derivation of aerosol properties from satellite measurements of backscattered ultraviolet radiation: Theoretical basis, *J. Geophys. Res.*, *103*(D14), 17,099–17,110, doi:10.1029/98JD00900.

Torres, O., P. K. Bhartia, J. R. Herman, A. Syniuk, P. Ginoux, and B. Holben (2002), A long term record of aerosol optical depth from TOMS observations and comparison to AERONET measurements, *J. Atmos. Sci.*, *59*, 398–413, doi:10.1175/1520-0469(2002)059<0398:ALTROA>2.0.CO;2.

Torres, O., A. Tanskanen, B. Veihelmann, R. Braak, J. P. Veefkind, P. F. Levelt, P. K. Barthia, C. Ahn, and C. Seftor (2007), Aerosols and surface UV products from OMI observations: An overview, *J. Geophys. Res.*, *112*, D24S47, doi:10.1029/2007JD008809.

Uematsu, M., A. Yoshikawa, H. Muraki, K. Arao, and I. Uno (2002), Transport of mineral and anthropogenic aerosols during a Kosa event over East Asia, *J. Geophys. Res.*, *107*(D7), 4059, doi:10.1029/2001JD000333.

Uno, I., H. Amano, S. Emori, K. Kinoshita, I. Matsui, and N. Sugimoto (2001), Trans-Pacific yellow sand transport observed in April 1998: A numerical simulation, *J. Geophys. Res.*, *106*(D16), 18,331–18,344, doi:10.1029/2000JD900748.

Voss, K. J., E. J. Welton, P. K. Quinn, R. Frouin, M. Miller, and R. M. Reynolds (2001), Aerosol optical depth measurements during the Aerosols99 experiment, *J. Geophys. Res.*, *106*(D18), 20,811–20,819, doi:10.1029/2000JD900783.

Wang, Z., and K. Sassen (2001), Cloud type and macrophysical property retrieval using multiple remote sensors, *J. Appl. Meteorol.*, *40*, 1665–1682, doi:10.1175/1520-0450(2001)040<1665:CTAMPR>2.0.CO;2.

Welton, E. J. (1998), Measurements of aerosol optical properties over the ocean using sunphotometry and lidar, Ph.D. dissertation, 150 pp., Univ. of Miami, Coral Gables, Fla.

Welton, E. J., et al. (2000), Ground-based lidar measurements of aerosols during ACE-2: Instrument description, results, and comparisons with other ground-based and airborne measurements, *Tellus, Ser. B*, *52*, 636–651, doi:10.1034/j.1600-0889.2000.00025.x.

Welton, E. J., et al. (2001), Global monitoring of clouds and aerosols using a network of micro pulse LIDAR systems, *Proc. SPIE Int. Soc. Opt. Eng.*, *4893*, 151–158.

Winker, D. M., W. H. Hunt, and M. J. McGill (2007), Initial performance assessment of CALIOP, *Geophys. Res. Lett.*, *34*, L19803, doi:10.1029/2007GL030135.

Young, S. A. (1995), Analysis of lidar backscatter profiles in optically thin clouds, *Appl. Opt.*, *34*, 7019–7031, doi:10.1364/AO.34.007019.

Zhang, L., M. Chen, and L. Li (2007), Dust aerosol radiative effect and influence on urban atmospheric boundary layer, *Atmos. Chem. Phys. Discuss.*, *7*, 15,565–15,580, doi:10.5194/acpd-7-15565-2007.

Zhang, X., S. Gong, Z. Shen, F. Mei, X. Xi, L. Liu, Z. Zhou, D. Wang, Y. Wang, and Y. Cheng (2003), Characterization of soil dust aerosol in China and its transport and distribution during 2001 ACE-Asia: 1. Network observations, *J. Geophys. Res.*, *108*(D9), 4261, doi:10.1029/2002JD002632.

Zhou, J., et al. (1998), Optical properties of aerosols derived from lidar measurements (in Chinese), *Chin. J. Quant. Electron.*, *15*, 140–148.

Zhu, A., V. Ramanathan, F. Li, and D. Kim (2007), Dust plumes over the Pacific, Indian, and Atlantic oceans: Climatology and radiative impact, *J. Geophys. Res.*, *112*, D16208, doi:10.1029/2007JD008427.

J. Bi, J. Huang, Z. Huang, J. Shi, G. Wang, and W. Wang, Key Laboratory for Semi-Arid Climate Change of the Ministry of Education, College Of Atmospheric Sciences, Lanzhou University, Lanzhou 730000, China. (hjp@lzu.edu.cn)

Q. Fu, Department of Atmospheric Science, University of Washington, Seattle, PO Box 351640, Seattle, WA 98195-1640, USA.

Z. Li, Department of Atmospheric and Oceanic Science, University of Maryland, College Park, MD 20742, USA.

S.-C. Tsay, NASA Goddard Space Flight Center, Greenbelt, MD 20771-0001, USA.